

Geophysical monitoring of large-scale levee overflow experiments with electrical resistivity tomography

Vana Tsimopoulou¹, Marios Karaoulis², Roeland Nieboer³, Edvard Ahlrichs⁴, André R. Koelewijn⁵ and Annette Kieftenburg⁶

Abstract

In the Interreg-funded Polder2C's project, large-scale overflow experiments were conducted from 2020 to 2022 on levee slopes along the Scheldt River in Belgium and the Netherlands. These tests assessed surface erosion resistance under varied conditions, including levee sections containing animal-induced damages. Electrical Resistivity Tomography (ERT) was employed as a non-invasive monitoring tool to observe subsurface changes, particularly those linked to erosion-prone animal burrows. A unique system configuration enabled detailed imaging of the levee's internal dynamics during overflow testing. Post-processed ERT data effectively captured subsurface changes during these events, including water infiltration into existing burrows, cavity formation and collapse, and the interconnection of subsurface voids.

The study demonstrates ERT's ability to identify critical subsurface features, with low resistivity zones indicating water-saturated areas and high resistivity zones marking air-filled voids. Time-lapse ERT imaging successfully captured dynamic resistivity shifts, correlating with key processes like soil displacement around burrows. Despite potential limitations, such as environmental noise and the influence of synthetic road plates used as protective coverings, ERT proved effective in detecting internal erosion patterns and pre-existing structural weaknesses.

The results indicate that ERT offers a feasible, scalable approach, also for real-time levee monitoring in overflow scenarios, enhancing its applicability for validation of erosion models. Future studies should investigate the effect of cumulative damage during overflow testing and optimize forms of data presentation to improve interpretability, ultimately refining ERT's potential as a reliable tool for predicting levee vulnerabilities.

Keywords

Levees, Overflow, Erosion resistance, Internal erosion, Animal burrows, Geophysical techniques.

¹ v.tsimopoulou@hz.nl, HZ University of Applied Sciences, Netherlands

² mkaraoulis@geo.auth.gr, Aristotle University of Thessaloniki, Greece

³ Roeland.Nieboer@deltares.nl, Deltares, Netherlands

⁴ Edvard.Ahlrichs@deltares.nl, Deltares, Netherlands

⁵ Andre.Koelewijn@deltares.nl, Deltares, Netherlands

⁶ a.kieftenburg@brabantsedelta.nl, Regional Water Authority Brabantse Delta, Netherlands

Research Article. **Submitted:** 13 November 2024. **Reviewed:** 11 December 2024. **Accepted** after double-anonymous review: 25 January 2025. **Published:** 28 February 2025.

DOI: 10.59490/jchs.2025.0041

Cite as: Tsimopoulou, V., Karaoulis, M., Nieboer, R., Ahlrichs, E., Koelewijn, A., & Kieftenburg, A. Geophysical monitoring of large-scale levee overflow experiments with electrical resistivity tomography. *Journal of Coastal and Hydraulic Structures*. Retrieved from <https://journals.open.tudelft.nl/jchs/article/view/7911>



The Journal of Coastal and Hydraulic Structures is a community-based, free, and open access journal for the dissemination of high-quality knowledge on the engineering science of coastal and hydraulic structures. This paper has been written and reviewed with care. However, the authors and the journal do not accept any liability which might arise from use of its contents. Copyright ©2025 by the authors. This journal paper is published under a CC-BY-4.0 license, which allows anyone to redistribute, mix and adapt, as long as credit is given to the authors. 

ISSN: 2667-047X online

1 Introduction

Earthen levees are critical components of flood defense systems and are widely used to protect coastal and riverine areas around the world (Sharp et al. 2013, Hughes 2011, Le et al. 2010). In densely populated regions like the Netherlands, these levees are thousands of kilometers long, safeguarding millions of people. The maintenance and upgrade of these levees are therefore vital to national safety (Government of the Netherlands, 2022). Numerous studies are conducted every year that contribute to continuous improvement of this practice. One of the topics of interest is to improve understanding and prediction of levee behaviour under extreme loading, such as a superstorm or prolonged periods of high water levels. This can reduce uncertainty in models describing physical processes that take place when different failure mechanisms are manifested, providing insights for assessing the risk of levee failures and setting priorities in life-cycle maintenance efforts.

One of the most effective methods for reducing uncertainty in such models is through in-situ levee stress tests. These simulations replicate extreme loading conditions on levees, allowing researchers to directly observe and assess their responses under realistic stress scenarios, and providing useful information for model validation (see e.g. Davies et al., 2010; Victor et al., 2011, 2012). Opportunities for such in-situ tests are scarce, especially for tests that can be continued beyond the onset of damage. On top of that, such levee stress tests can be costly and logistically challenging. For this reason, when an opportunity arises to perform such tests, researchers strive to measure as many parameters as possible. Detailed measurement plans are developed in advance, which for overflow and overtopping experiments usually include the measurement of hydraulic parameters, such as flow velocities and water depths, and surface erosion parameters, such as erosion rates and scouring depths (Hoffmans et al., 2008; Steendam et al., 2013; Ponsioen et al., 2019; Nicaise et al., 2023), or failure mechanisms occurring deeper in the levee (Zwanenburg et al., 2012; Koelewijn et al., 2014; Lengkeek, 2022).

A unique opportunity to conduct large-scale overflow and wave overtopping tests emerged along the Scheldt River, on the border between Belgium and the Netherlands, as part of a flood protection and nature development plan, the so-called Sigma Plan (Bulckaen et al., 2006). Since a number of levees were slated for removal, extensive testing was possible under an Interreg-funded project so-called Polder2C's (www.polder2cs.eu). These tests, conducted over two winter seasons (2020-21 and 2021-22), provided valuable data on levee performance under simulated extreme loading.

The testing plans were designed to assess various factors, such as different grass lengths, soil types, and the presence of anomalies like trees and animal burrows. Additionally, the performance of emergency measures like mobile barriers and protective coverings was evaluated (Depreiter & Peeters, 2020; Depreiter & Peeters, 2021). The large number of tests allowed researchers to refine experimental setups, improve measuring techniques, and explore novel approaches that could benefit future in-situ testing. Within this context, a new setup for geophysical monitoring using Electrical Resistivity Tomography (ERT) was developed and applied for the first time during an overflow experiment, resulting in a timelapse of the developments underneath the surface. This paper presents this innovative setup, the data it provided, and its potential application in the development and validation of internal erosion models.

The overflow experiment where the new setup was installed, took place on a 2m-wide levee section where an extensive system of mole burrows had been detected previously. The presence of the burrow system was the basic reason for the selection of the section. Prior to this, two overflow tests elsewhere in the project area, unexpectedly led to failure, caused by the presence of mole burrows, urging project researchers to emphasize the study of animal-induced anomalies in later tests. Hence this later test aimed primarily at improving knowledge about the influence and management of animal burrows on levees. As explained before, secondary objectives were set per experiment to improve the quality of future in situ experiments, and this section was no exception. The primary and secondary objectives of the test were (Tsimopoulou & Koelewijn, 2023):

- 1) Test the feasibility and effectiveness of a low-cost technique for temporary protection of the levee containing a mole burrow system with the use of road plates (primary objective).
- 2) Test the feasibility of electrical resistivity tomography (ERT) as a technique for monitoring the influence of overflow in subsurface erosion during overflow testing.
- 3) If ERT proved feasible, monitor internal erosion patterns through observation of the evolution in the geometry of burrows during overflow.

- 4) Compare the results of the ERT scans with ground penetrating radar (GPR) scans at the same location.
- 5) Refine the inspection of animal burrow systems on levees with a so-called smoke experiment.

The second and third item in the above list (both secondary objectives) coincide with the scope of this paper. The first item (primary objective) is out of the scope of this article, but it is briefly discussed here, since the presence of road plates influenced our experimental setup and the results of the ERT measurements. The last two items (secondary objectives) are not discussed here. The smoke experiment is detailed by Keirsebelik et al. (2024).

2 Underlying principles and knowledge

2.1 Large-scale levee experiments and animal burrows

Large-scale overflow experiments on levees have been carried out several times over the past few decades, as described e.g. by Whitehead & Nickersons of Rothwell (1976), Cantré et al. (2017) and Nicaise et al. (2023). While overflow comprises a continuous flow over the landside slope of the levee, wave overtopping results in a discontinuous flow. Wave overtopping tests have been carried out at various locations in the Netherlands, Belgium, and Vietnam since 2007 (Van der Meer et al., 2010; Le et al., 2011). For these tests, generally a levee section is selected with a good grass quality, showing no defects in a quick visual inspection.

An analysis by Van Dijk (2021) considering 32 test sections from 11 locations distributed across the Netherlands and Belgium, showed that in roughly half of the sections, mole burrows were present. In most cases, these burrows had a negative outcome on the resistance of the levee to wave overtopping conditions. In some cases, animal burrows actually lead to failures of levees. Examples of levee failures attributed to burrowing animals are given by Bayoumi & Meguid (2011), Orlandini et al. (2015), Taccari (2015), Camici et al. (2017), Saghaee et al. (2017), and Ceccato & Simonini (2023).

2.2 Electrical properties of the subsurface

The electrical resistivity of the subsurface is a fundamental property that reflects the ability of materials beneath the Earth's surface to impede the flow of electric current. This property varies across different geological materials, forming the basis for geophysical exploration and environmental assessments. The parameters that have the greatest influence are moisture content, followed by material composition. More specifically, the presence and distribution of water in the subsurface has a profound effect on electrical resistivity. Saturated soils conduct electricity more effectively than dry materials, influencing resistivity measurements. An important parameter here is the quality of the water content (i.e. fresh, salt) which dictates the overall resistivity value of the soil.

Different geological materials exhibit distinct resistivity values. Rocks and minerals typically have higher resistivities, while soils and water display lower resistivities. The mineral content and porosity of the subsurface significantly impact resistivity (Table 1). In our experiment, both the water quality and mineral composition remain stable, thus the resistivity values, or better, the changes we observed in the resistivity values originate from changes in the in the moist content on the porosity.

When air-filled holes are present in the ground, they will appear as resistive targets. Even though air has infinite resistance, the current flows in 3D sense in the subsurface and therefore the presence of a cavity will increase the resistivity value in contrast to soil without holes. Yet it will not reach an infinitely high value. The exact value depends on many parameters, mainly on the size and location (in 3D) of the cavity. This analysis is not part of this work since data were collected in 2D sense. Cavities will appear as resistive targets, with higher value than the surrounding. The behaviour of the soil (and cavities) during the overflow experiment can be categorized in four types:

- 1) The cavity is filled with water, so we will see a decrease in resistivity at this specific location.
- 2) The cavity will remain with air and will enlarge during the experiment, signifying subsurface erosion. Here we will see a high increase in resistivity value.

- 3) New cavities can be created that can be filled with water.
- 4) New cavities that are created empty again.

Table 1: Electrical properties of subsurface material (Adapted from Rosas Carbajal, 2014).

Subsoil material	Resistivity [Ωm]	
	Lower bound	Upper bound
Clays	1	100
Sand	4	800
Loam	5	50
Marl	3	70
Consolidated Shale	20	2000
Gravel/Conglomerate	2000	10000
Coarse grained Sandstone	10	96000
Siltstone	1	15000
Sandstone	50	8000
Limestone	80	1000

2.3 ERT rationale and application in levee investigations

Electrical Resistivity Tomography (ERT), also known as electrical resistivity imaging (ERI), is a geophysical technique used to visualize subsurface structures and variations in electrical resistivity. It is commonly applied in environmental studies, geotechnical investigations, archaeology, and mineral exploration. The ERT setup involves placing a series of electrodes in the ground. Typically, a current is introduced into the ground through two electrodes, and potential differences are measured between other pairs of electrodes. Electrical current flows through the subsurface, and the potential differences are recorded. The measurements are collected for various electrode configurations (i.e. arrays) to create a comprehensive dataset. The collected data are then processed through a mathematical technique called inversion. Inversion algorithms use the measured data to estimate the distribution of electrical resistivity in the subsurface. The result of the inversion is an electrical resistivity model, often represented as a two-dimensional or three-dimensional image. For more information on the ERT set up, the reader is referred to Revil et al. (2012). When data are collected over time, they can be processed with the time component by using time-lapse algorithms (Karaoulis et al., 2013). This means that in principle, all necessary tools for imaging the behaviour of animal-induced cavities on a levee before, during and after a large-scale stress test are available.

In levee investigations, ERT proves to be a useful technique in static surveys of the subsoil. That is the mapping of soil properties in the entire levee subsurface at a specific moment in time. This is done with the provision of 2D- or 3D-images with detailed values of the electrical properties in the entire levee body (see example in Figure 1). This allows the detection of various types of anomalies, such as cavities created by animals, as well as changes in the consistency and the water content of the subsoil (see e.g. Antoine et al., 2022). In overflow tests, ERT is typically only used for characterization prior to testing. Data collection during testing or even a re-analysis right after it has not been reported in literature so far.

The most prominent advantage of ERT is its non-destructive nature, making it a valuable tool for imaging the subsurface without the need for drilling or excavation. However, the resolution and accuracy of the results depend on factors like the electrode spacing, depth of investigation, and the specific geological conditions of the survey area. Although ERT has been described as a preferred and widely applied technique for levee surveys, it does have limitations that may reduce the scope of its application. As the method requires the introduction of an electrical current, disturbances may occur in the collected datasets by the presence of metal objects like pipes and sheet piles, temperature differences, rainfall and 3D effects (Dezert et al., 2019).

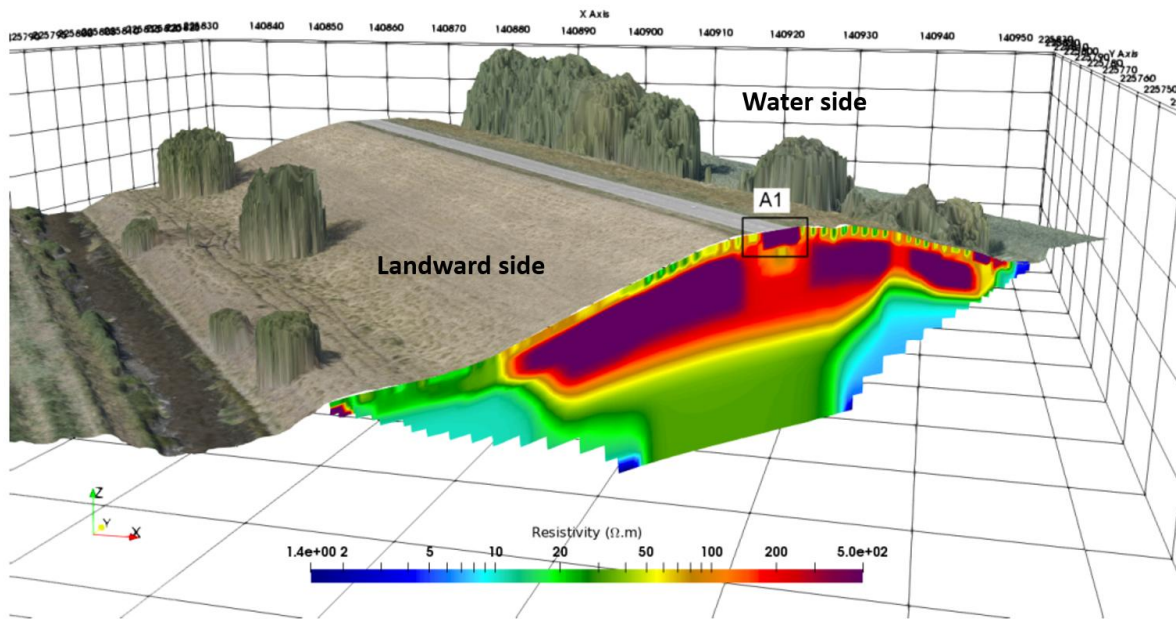


Figure 1: 2D-image of electrical resistivity integrated in a spatial elevation model of the Prosperpolder levee in Belgium. The colourbar indicates resistivity values. (Copied from: Antoine et al., 2022 with the authors’ consent).

3 Methodology

3.1 Test location

The tests described here were carried out on the landside slope of the levee of the Hedwigepolder along the left bank of the Scheldt River. That is approximately 19 km downstream of Antwerp past the Belgian-Dutch border, hence in the Netherlands (Figure 2, left). This was a levee within the boundaries of the so-called Living Lab Hedwige-Prosperpolder, which was the test area of Polder2C’s.



Figure 2: Left: Map indicating the location of the overflow experiment (Background image source: Google Earth); Right: Aerial impression of the 3-km-long levee of the Living Lab Hedwige-Prosperpolder, where the overflow experiment took place. The red line marks the crest of the levee. (Source: Tsimopoulou et al 2022).

The living lab was created in 2020 in a Dutch-Belgian cross-border site, where a managed realignment project was in progress. The living lab consisted of a 3 km-long earthen levee that was breached in 2023 to facilitate the expansion of an adjacent intertidal area (Figure 2, right). Since the levee was bound to be removed while it was still in a good condition because of its regular maintenance till that point in time, researchers had the opportunity to perform large-scale

experiments with superstorm conditions. These could potentially lead to catastrophic failures. The tests took place after the local water authorities safeguarded safety of the region by building a new levee further upland.

The exact test section was selected after a thorough investigation of a 100 m long levee stretch on the presence of mole and vole burrows (Tsimopoulou & Koelewijn, 2022). Various other overflow and overtopping experiments were scheduled for the same experimental season, whose locations are highlighted in Figure 3. The levee at this spot has a landside slope of about 21° or approximately a 3V:8H slope, and its cross-section consists of a sandy core covered by a clay layer of 80-100 cm (Figure 4a). The selection of the test location for the installation of ERT was determined by the distribution and characteristics of the surveyed animal burrows. The chosen section was of particular interest because it contained several mole burrows, nine of which were interconnected underground (Figure 4b). To confirm the interconnectedness of these burrows, a "smoke experiment" was conducted. This involved introducing coloured smoke into one burrow entrance and observing its emergence from neighbouring burrows (Keirsebelik et al., 2024). Sections of levees with interconnected cavities in the subsoil are considered more vulnerable when subjected to overflow and / or overtopping conditions, although there are no studies that clarify specific load parameters that the cavities are most vulnerable to.

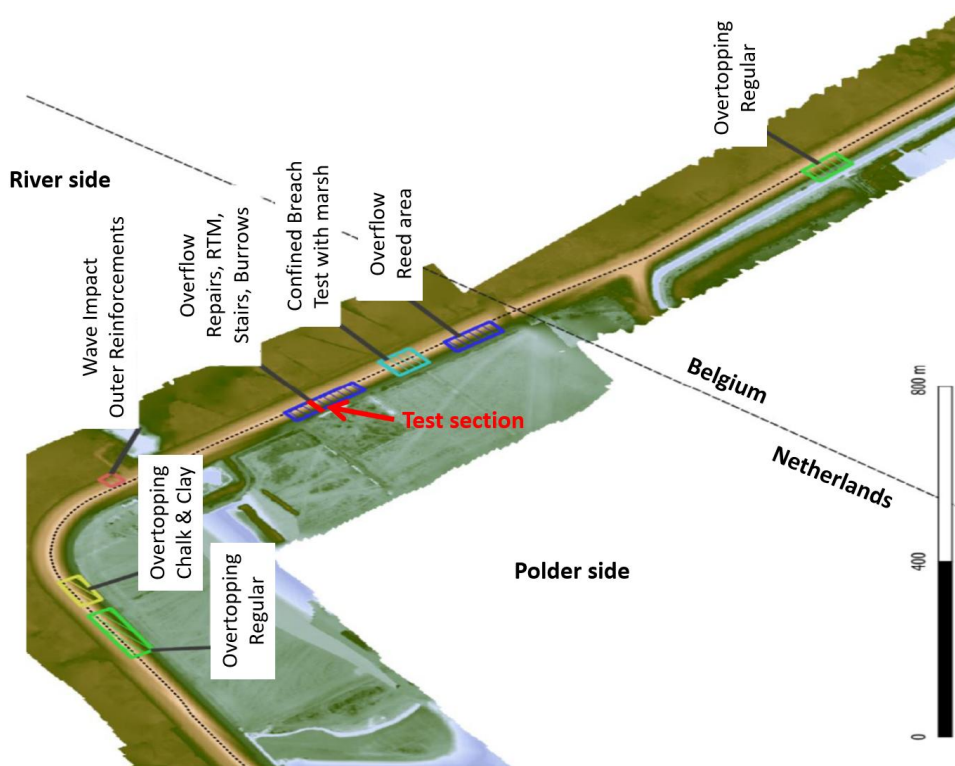


Figure 3: Digital terrain model of the Living Lab Hedwige Prosperpolder highlighting the large-scale levee stress tests from Polder2C's second experimental season. The specific test section with ERT installation is marked in red (Adapted from: Depreiter & Peeters, 2021).

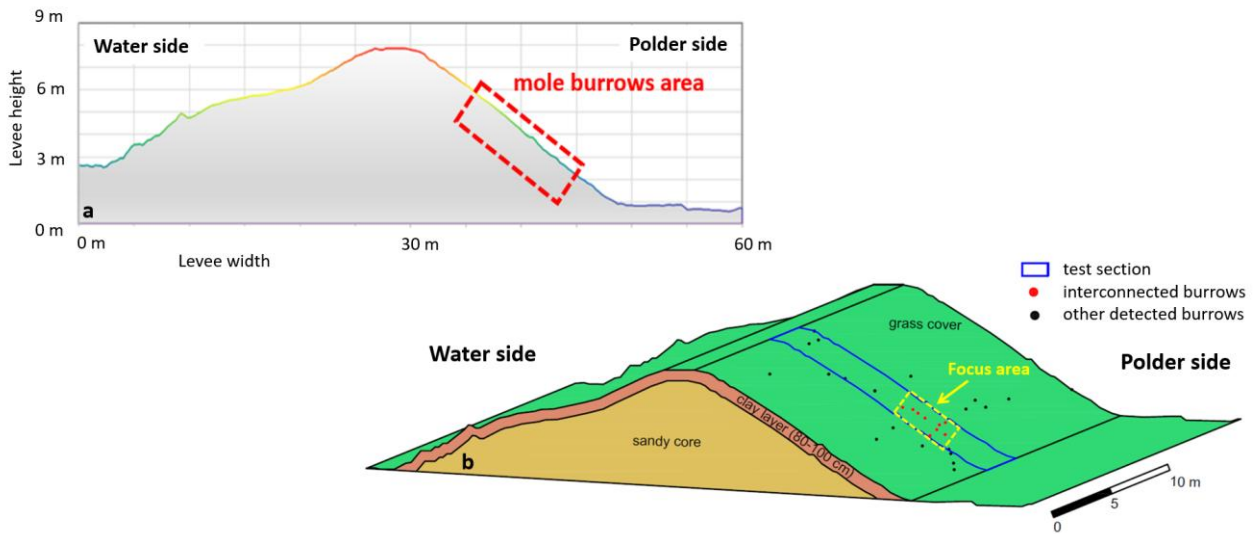


Figure 4: Levee cross-section at the test location in 2D and 3D featuring the cross section geometry and materials, the spread of mole and vole burrows on a levee stretch of 20m, the interconnected mole burrows and the test section. The colours at the outline of the 2D cross-section correspond to the levee height.

Given the available ERT measurement equipment, and in particular the available number of sensor and the length of cables (see also sections 3.2 and 3.3), the part of the test section with interconnected burrows was prioritized as a focus area for the ERT monitoring.

3.2 Experimental set-up

The overflow generator developed by Flanders Hydraulics Research forms the basis of the experimental setup. This has been designed to uniformly distribute water over a dike crest for overflow experiments. It consists of three components made of high-density polyethylene, a base, a reservoir, and a bridge. Their compact shapes and lightweight material allow for easy transport and assembly. Water is pumped through an inlet structure into the generator, where it flows over a bridge onto the dike crest and down a flow canal lined with coated hardboard plates. Sensors and cameras monitor the experiments (see also Figure 5). This system allows flows up to 66 m³/min over a 2 m wide section, which equals to 33m³/min/m or 0.55m³/s/m. To prevent water leakage and erosion during testing, EPDM sheets and sandbags are applied at vulnerable spots. For a detailed description of the overflow generator, the reader is referred to Koelewijn et al. (2022).



Figure 5: Impressions of the various components of the overflow generator (Source: Polder2C’s archive, www.polder2cs.eu).

For this specific experiment, the flume was installed with a width of 2 m (see exact position in Figure 4b). This was a standard width that was used in the majority of Polder2C’s experiments. Since the primary goal of the overflow experiment was to test the feasibility and effectiveness of a low-cost emergency measure against surface erosion, a part of the focus area within the flume was covered with road plates. In particular the road plates were installed in a configuration that covered all the interconnected mole burrows. To enable ERT measurements at the same location, synthetic road plates were applied instead of metal ones. This was necessary as metal objects can undermine the quality of ERT imaging. A clear practical advantage of these synthetic road plates when used as an emergency measure is that they are much lighter than metal ones, allowing to have them placed by two people without the need of additional heavy equipment. This makes them easily deployable in various locations even under adverse weather conditions. The road plates were fixed on the slope by metal pins. Their exact positioning and configuration in the flume is shown in Figure 7.



Figure 6: Impression of the location and configuration of the road plates in the flume and the types of pins that were used for their attachment to the ground (Source: Tsimopoulou & Koelewijn, 2023).

To measure and monitor the changes in the subsurface during overflow, two parallel cables were installed on the slope of the levee, see Figure 7 (left). The installation of the electrodes was planned to match the interconnected mole burrows. Since the area of interconnected mole burrows was selected as the most interesting for the subsoil measurements, it was deemed suitable to place the ERT electrodes as close as possible to the cavities, hence underneath the road plates, which were meant to cover the cavities in any case. For this reason the ERT electrodes were installed in the flume prior to the application of the road plates. Cable 1 was covered by the synthetic road plates, while cable 2 was on open soil. The main goal was to measure below the plates, and cable 2 was installed mainly as a backup in case cable 1 failed. From cable 2 data were collected only before and after the end of the experiment. This choice was purely dictated by the acquisition time required for each measurement. Doubling the number of pins would approximately double the acquisition time, as the time depends heavily on the array used and the number of deployed pins. To achieve the highest frequency of measurements during the overflow experiment, we prioritized cable 1.

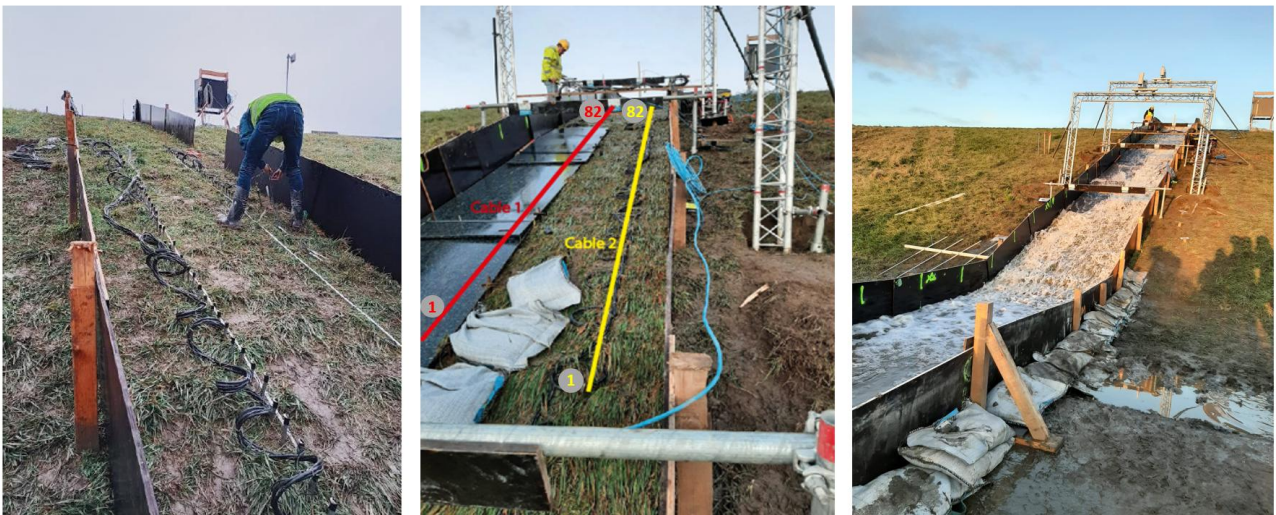


Figure 7: Installation of the second ERT cable (left), configuration on the slope during no-flow period (middle), flow in the flume (right).

164 electrodes were utilized in total with 10 cm long stainless steel pins pushed into the ground, see Figure 7 (left). The cables used in this experiment were developed by Deltares. The exact cable configuration and their connection to the data acquisition system is illustrated in Figure 8. The measuring array was optimized for short time acquisition, and it contained a selection of dipole-dipole array and gradient array. The electrode spacing was 10 cm, yielding a horizontal resolution of at least 5 cm. This means that the smallest geological structure or resistivity anomaly that can be accurately detected and represented in the resulting model is approximately 5cm. The optimization is based on the sensitivity matrix, which means that only the best measurements were kept for each discretization cell.

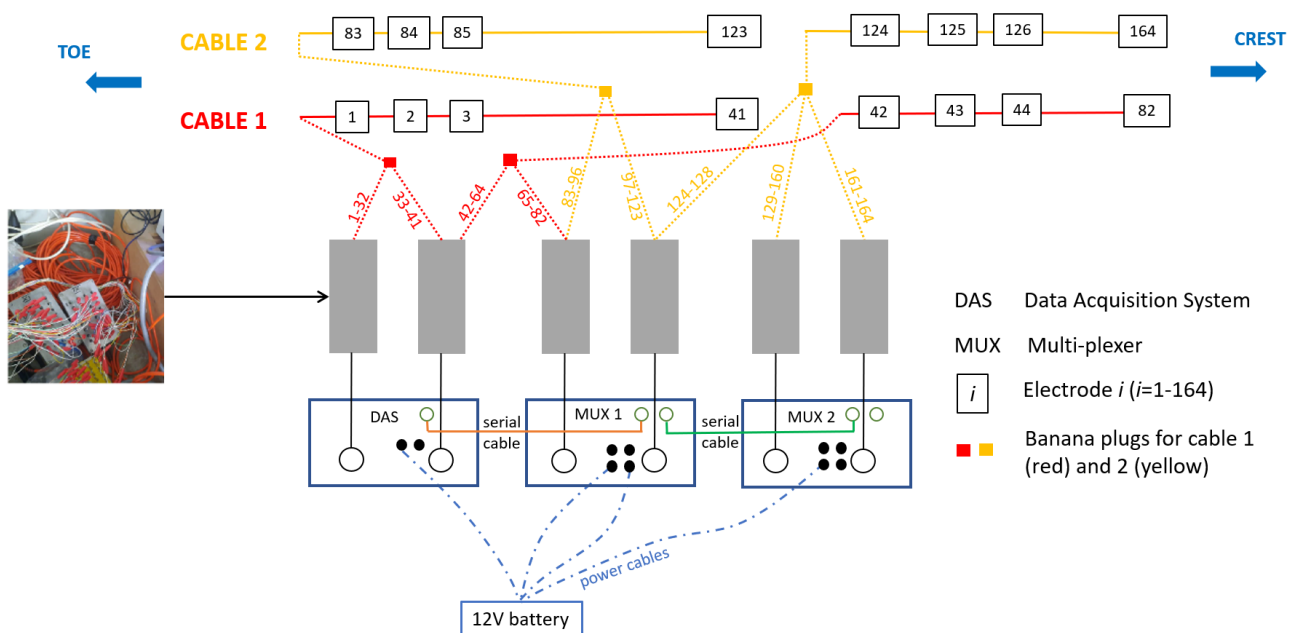


Figure 8: Detailed sketch of cable configuration used in this experiment and their connection with the data acquisition system.

3.3 Data acquisition

In total four overflow test runs were conducted, with increasing flow discharges, during which ERT measurements were taken. ERT measurements were taken at regular intervals to monitor changes in resistivity as an indicator of internal erosion and soil displacement. Prior to this, a first reference ERT scan was made for calibration of the system. As

explained in the previous section, from cable 1 that was placed under the road plates, data were acquired before, during and after the overflow test runs, i.e. in all measurement intervals. Cable 2 has data right before and after each overflow test run.

For the data acquisition, the subsurface was discretized in layers parallel to the levee surface with thicknesses of 3 to 8cm. Two different acquisition protocols (arrays) were utilized to capture distinct features in the datasets. In the first protocol the focus was on minimizing time intervals between consecutive measurements to capture temporal changes more efficiently, although this resulted in a shallower depth of investigation. In contrast, the second protocol prioritized depth of investigation, allowing for resistivity measurements at greater depths but requiring longer acquisition times. The two protocols are listed below:

- Protocol 1 - ‘Shallow’: The depth of investigation is 0.26m (discretization is based on unstructured triangle mesh, where we fixed the maximum element area size of 25cm² and 3 nodes between two sequential electrodes), the time interval is 3min between two sequential rounds. This protocol was meant to capture as many time-related changes as possible.
- Protocol 2 – ‘Deep’: The depth of investigation is 0.6m (similar mesh settings), the time interval is 10min. This protocol meant to capture deeper parts of the model (in expense the longer time-interval).

During the first overflow test, the team used the "shallow" protocol, which focused on frequent measurements in the top 26 cm of the surface. In the second test, we began with the same shallow protocol but switched to the "deep" protocol for the final four measurements due to an unexpected interruption; one of the team members tested positive for COVID-19, requiring the test to pause indefinitely. Faced with uncertainty about whether we would be able to resume the experiment after the COVID-19 alert, we decided to switch to the deep protocol to evaluate its performance and collect preliminary data at greater depths. This decision allowed us to take advantage of the available time to explore the utility of the deep protocol, as we could not be certain that the experiment would continue. Fortunately, after a three-day break, the tests resumed, and the final two runs were completed using the deep protocol. These later tests provided valuable insights into subsurface processes at greater depths.

The data acquisition plan was designed to present the ERT measurements in two ways: as absolute resistivity values and as ratio images showing changes in resistivity over specific time intervals, particularly during each overflow test run. The goal was to make the results clear and easy to understand not only for geophysicists, who are experienced in interpreting resistivity data, but also for levee experts who might not be as familiar with geophysical methods. To achieve this, the plan included taking reference ERT measurements before and after each test run, when the flow was stopped, so there would be clear points of comparison. This plan was followed in all the test runs except the third one (i.e. ERT experiment 4), where an initial reference measurement was missed due to an unintentional timing oversight by the field crew. This reduced the capacity of the team to comprehensively interpret the acquired results of this specific experiment (see also section 4).

An overview of the test runs with their corresponding flow discharges, duration and the associated ERT measurement is presented in Table 2.

Table 2: Overview of overflow test runs and associated ERT measurement number.

Overflow test run	ERT experiment	Flow discharge [m ³ /min]	Duration [min]	Protocol	Total measurements	Measurement during flow	Remarks
[-]	1	0	0	1	1	0	Calibration, no flow. Data to be used in the validation stage.
1	2	5.6	32	1	15	13	[-]
2	3	5.8	40	1&2	11	9	7 measurements in Protocol 1 and 4 measurements in Protocol 2

3	4	9.0	43	2	6	5	No initial measurement before flow started.
4	5	12.0	40	2	6	5	[-]

3.4 Data processing

The collected data were the potential differences between transmitting and receiving electrodes, which are influenced by the subsurface resistivity distribution, i.e. the key property being investigated. The steps in the data processing workflow needed to ensure that the subsurface resistivity was accurately reconstructed, with high-quality data and minimal error. In order to achieve the best-fitting resistivity model for interpretation, a combination of a mathematical optimization, i.e. the so-called inversion process, with geophysical plausibility checks was performed. This is a commonly used approach in ERT data processing (see e.g. Loke, 1994; Loke & Dahlin, 2002).

The first step was to control the quality of data through identifying and filtering out erroneous measurements, which could have arisen from issues like electrical noise or poor electrode coupling with the ground. Filtering is a complex procedure, particularly when working with time-lapse data, as there is no straightforward automated way to remove bad data points. A geophysicist is always needed to assess and address several potential sources of error, including 1) errors from bad pin connections (i.e., poor coupling with the ground), 2) random errors from the measuring system, and 3) errors originating from modeling. The process is inherently iterative, requiring expertise and careful consideration at multiple stages. For more details, readers can refer to relevant studies such as Karaoulis et al. (2011, 2014). Erroneous data points, such as unusually high or low values, were removed to ensure optimal data quality. For instance, in Line 1, data from pin number 20 were excluded due to unusually high contact resistance, likely caused by a bad wire connection.

In preparation of the inversion process, a so-called forward modeling was performed, which involved simulating how the subsurface might respond electrically, based on a given resistivity distribution. Essentially, forward modeling calculates the predicted voltage readings at the surface, assuming a known resistivity model. Next the inversion process takes place. This is a mathematical technique used to reconstruct the subsurface resistivity from the voltage measurements collected during a survey. The goal is to find the best resistivity model that explains the observed voltage data. This is done by adjusting the resistivity values within the model until the calculated voltages match the actual measurements. The inversion process is iterative, meaning that with each step, the resistivity model is refined, and the forward modeling is recalculated, gradually improving the fit between the predicted and observed data. To avoid overfitting and ensure realistic results, regularization techniques are often applied during inversion (Karaoulis et al. 2013). Regularization helps stabilize the solution, smoothing the resistivity model while balancing data accuracy and preventing unrealistic features. The quality of the inversion results depends on several factors, including the electrode configuration, the quality of the measured data, and the regularization settings. Inversion results also carry some level of uncertainty, which should be considered when interpreting the final resistivity model. The inversion process was conducted using the PyGIMLI software (Rücker et al., 2017), which enabled the assessment of different inversion options. For example, applying smoothing helped regulate the sharpness of transitions between layers. After analyzing the inversion results, common features were identified, providing confidence in the interpretation of the subsurface resistivity structure.

Once the inversion process was complete, the resulting model needed to be evaluated for geological and geophysical plausibility. The final resistivity model was assessed for how well it represented the subsurface structures, considering the resolution limitations imposed by the inversion parameters. The model’s accuracy was judged by the Root Mean Square (RMS) misfit between the predicted and measured data. For Line 1, the final RMS misfit was under 3%, indicating high-quality results. For Line 2, where no data was excluded, the RMS error was also below 3%.

While the RMS misfit quantifies the spread in the model, it does not capture potential biases. To avoid bias in the model, this work used a starting model of a homogeneous half-space. Although prior studies have shown that the final results can often improve when a prior model is used, we chose not to apply such a model here. Another potential source of bias is the regularization parameter, which influences the smoothness of the resistivity distribution. The effects of different regularization parameters on resistivity inversion have been studied extensively in the literature (see e.g. Karaoulis et al. 2011; 2014), and these findings were considered in the interpretation of our results.

4 Results

4.1 Spectrum of resistivity values and recorded features

The resistivity measurements recorded before the testing started and after each test run (as part of the ERT experiments listed in Table 2-referred to as experiments in the following sections) are shown in Figure 9. The first two graphs, (a) and (b), display the data taken before testing began and after the completion of experiment 2, but only go to a depth of 26 cm. This is because the measurements were made using protocol 1, which focused on the top 26 cm of soil. Starting midway through experiment 3, we switched to protocol 2, which allowed measuring resistivity down to a depth of 60 cm. As a result, the remaining graphs (c, d, and e), which show the data for experiments 3 to 5, capture measurements down to 60 cm, reflecting the deeper focus of protocol 2.

The resistivity values recorded during the experiments ranged from 2.6 $\Omega\cdot\text{m}$ to 55 $\Omega\cdot\text{m}$. Lower values, around 2.6 $\Omega\cdot\text{m}$, indicate areas of high water saturation, where the soil is fully soaked, and water fills the pores, making it more conductive. As we move away from these saturated zones, the soil becomes less waterlogged, and resistivity gradually increases. In these transitional areas, water content decreases, and air starts to fill some of the pore spaces, leading to higher resistivity. The highest resistivity values, around 55 $\Omega\cdot\text{m}$, suggest not only drier or less saturated soil but also the presence of air-filled cavities. Air is highly resistive, and its presence in drained or weakened areas of the soil significantly raises resistivity. Since other methods confirmed the existence of interconnected mole burrows in the same section of the levee, it is reasonable to conclude that the highest resistivity values reflect voids or cavities where water has drained out. While factors like soil type, pore water salinity, and soil compaction can also influence resistivity, these factors are less critical in this case. Fresh water was used for the overflow tests, so salinity isn't a significant factor, and the small size of the experimental flume makes large variations in soil compaction unlikely. Additionally, since the top 60 cm of the soil is in a clay layer (as shown in Figure 4b), with grass cover and roots present in the uppermost portion, their potential influence on resistivity is expected to be localized and minimal relative to the overall observed trends.

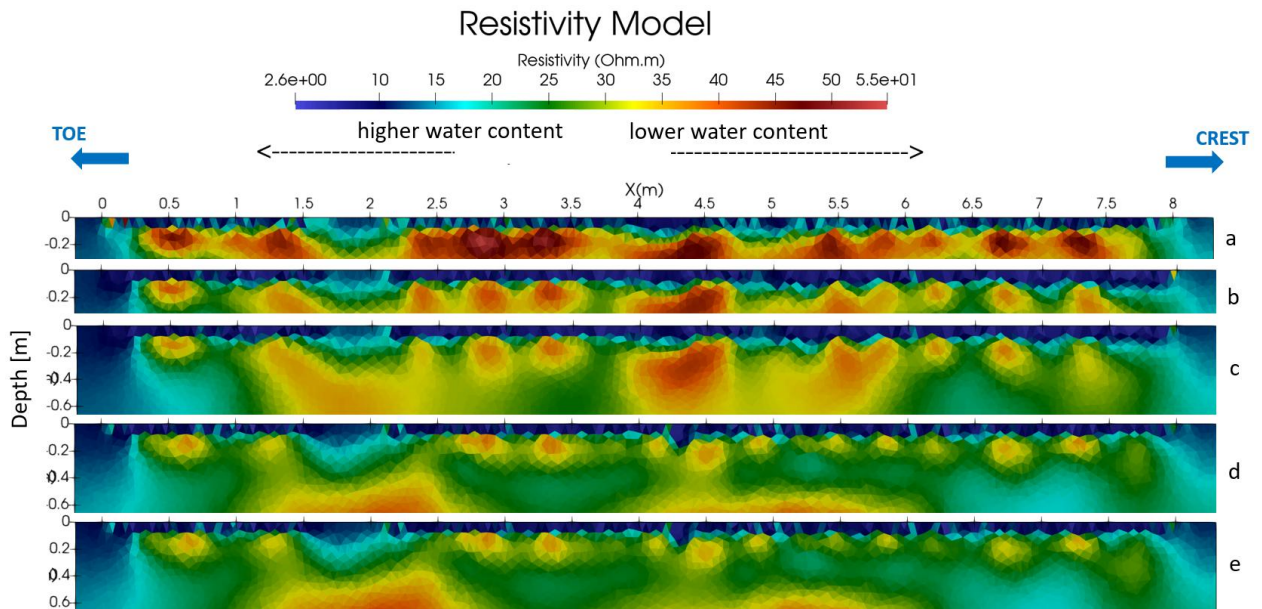


Figure 9: Recorded resistivities from cable 1 before initiation of testing (a) and after completion of experiments 2 (b), 3 (c), 4 (d) and 5 (e).

In all graphs of Figure 9, the top 10 cm of soil consistently show very low resistivity, indicating a layer of clay with high water content close to the surface, even before the experiment began. This is reasonable due to the rainy weather in the days leading up to the test. Pictures taken during the installation of the ERT electrodes (Figure 7, left) clearly show a wet levee slope with visible muddy patches, confirming these conditions. After the first overflow run (Figure 9b), the resistivity value below the surface layer drops significantly, indicating a highly saturated layer that remains waterlogged throughout the subsequent test runs (Figure 9c to 9e).

A notable feature in the resistivity scans, particularly in the 10–35 cm depth range, is the appearance of high resistivity values. In the pre-experiment scan (Figure 9a), the highest resistivity values in this depth range are observed at specific locations along the X-axis: $X = 0.5$ m, 1.3–1.5 m, 2.3–3.5 m, 4.3–4.5 m, 5.5 m, 5.7 m, 6.2 m, 6.7 m, and 7.3 m. These locations and depths align with the positions of mole burrows identified through ground-penetrating radar and visual probe inspections. Therefore, it is reasonable to conclude that these high resistivity areas represent the air-filled cavities of the mole tunnels. After each consecutive experiment, the resistivity at these spots gradually decreases, suggesting that water is infiltrating and filling the tunnels, possibly, some collapse has also taken place.

While this data provides valuable insights into how the cavities are evolving over time, the images in Figure 9 offer limited visual evidence of specific time-dependent processes. In accordance with the possibilities generally stated in Section 2.2, here four key processes are likely: (1) existing air gaps (mole tunnels) being filled with water, (2) the formation of new gaps in the subsurface, either filled with air or water, (3) the collapse of existing tunnels, and (4) tunnels beginning to connect with each other. To gain a clearer understanding of these processes, it is helpful to compare the resistivity graphs in Figure 9 with ratio images that show the degree of resistivity change over time (see Section 4.2 for more detail).

4.2 Results per experiment

Figure 10 to Figure 13 illustrate the ratio images of experiments 2 to 5. Experiment 1 refers to the initial calibration measurement without flow and is not presented here. The red areas in these images represent areas where resistivity increased in comparison to the image before the flow started, i.e. the graph of absolute resistivity values that is shown on the top of each figure, while the blue areas represent those areas where resistivity drops. The grey areas correspond to neutral zones, i.e. areas where resistivity remains stable.

In Experiment 2 (Figure 10), the initial overflow run with the lowest flow discharge of $q=5.6$ m³/min, the resistivity ratio images from $t=0$ to $t=16$ minutes reveal a significant increase in resistivity at specific locations: $X=1.7$ –2.1 m, $X=4.1$ –4.3 m and $X=4.9$ –5.1 m. These regions appear red on the images, indicating the development of new voids adjacent to the pre-existing mole cavities. From $t=20$ minutes onward, however, the red colour fades in these areas, suggesting that the initial void formation process gradually reverses, allowing soil to refill these spaces. This phenomenon is corroborated by the final absolute resistivity values after the flow ceases, as minimal resistivity changes are observed in the same locations, confirming that the voids largely fill back in.

In contrast, across the remaining lengths of the scanned surface, specifically at locations $X=0$ –1.7 m, $X=2.1$ –4.1 m, $X=4.3$ –4.9 m and $X=5.1$ –8 m, the blue coloration dominates from start to finish, indicating increased water content throughout these regions. Comparing these water-saturated areas with the absolute resistivity values prior to the flow (shown in the top image of the figure), the darkest blue regions are observed around the peripheries of the pre-existing mole cavities described in Section 4.1, while the cavities themselves appear pale blue. This pattern indicates that infiltration occurs primarily around the cavities, while the cavities themselves remain relatively intact, with only small amounts of water infiltrating them.

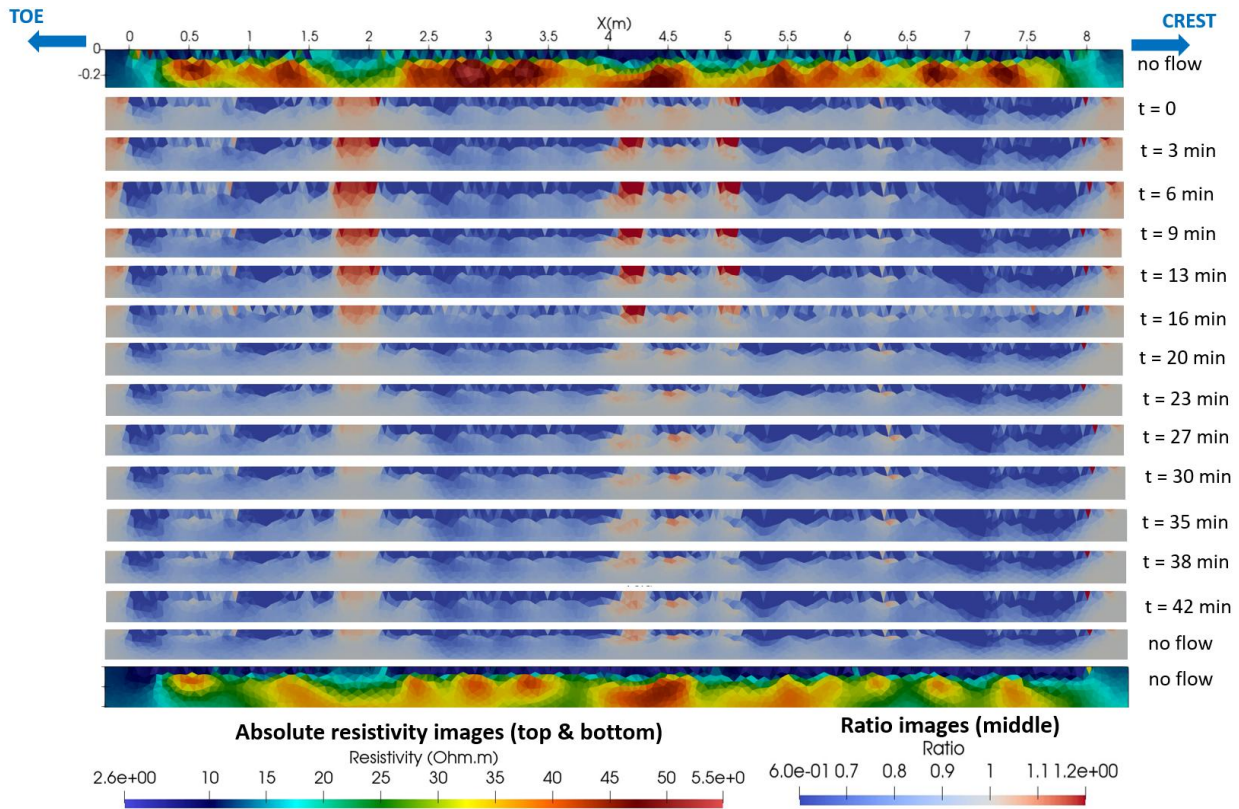


Figure 10: Measurements for experiment 2, cable 1.

Experiment 3 (Figure 11), conducted on the same day with a slightly increased flow discharge of $q=5.8 \text{ m}^3/\text{min}$, largely replicates the patterns observed in Experiment 2, with minor differences. Here, red regions reappear at the same locations where new voids developed in Experiment 2, but this time, these red areas persist through the end of the experiment, indicating that the voids remained open after reforming. As in Experiment 2, the darkest blue regions appear adjacent to the pre-existing cavities, while the cavities themselves display a gray (e.g., $X=4.3-4.6 \text{ m}$) or pale blue (e.g., $X=7.3 \text{ m}$) hue. In the former, this shows the cavities remain intact, whereas the latter suggests gradual filling with soil particles, likely driven by the pressure exerted by water-saturated soils in adjacent areas toward these lower-pressure cavities.

A novel phenomenon observed in Experiment 3 is the appearance of high-resistivity spots near the surface in the $t=6 \text{ min}$ ratio image, at locations $X=0.3-1.5 \text{ m}$, $X=2.5-2.7 \text{ m}$, $X=3.5-4 \text{ m}$ and $X=6.3-8 \text{ m}$. These spots gradually diminish in subsequent images, indicating initial surface erosion likely due to the formation of small voids as surface grass is uprooted or displaced. Notably, no significant resistivity changes were recorded at greater depths after switching to the ‘deep’ data acquisition protocol at $t=20 \text{ min}$, indicating that, at this moderate flow discharge of $5.8 \text{ m}^3/\text{min}$, the overflow test had minimal impact on deeper zones.

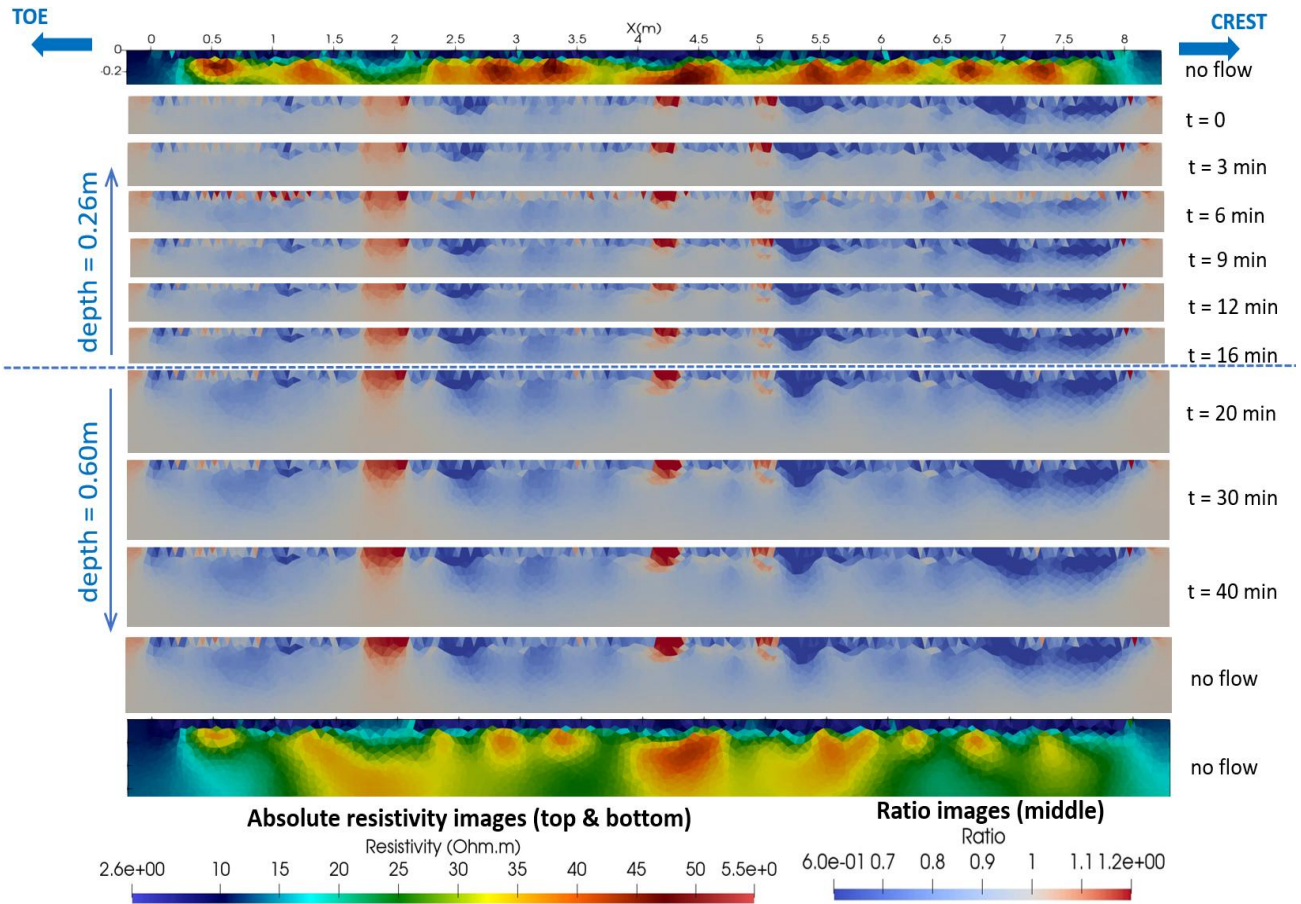


Figure 11: Measurements for experiment 3, cable 1.

Experiment 4 (Figure 12) was conducted three days after Experiment 2, with an increased flow discharge of $q=9 \text{ m}^3/\text{min}$. Unlike previous experiments, baseline resistivity values were not recorded before flow initiation due to measurement oversight, so ratio images in Figure 12 use the resistivity values at $t=0 \text{ min}$, just after flow started on the levee slope, as a reference. This adjustment leads to notable differences in resistivity patterns compared to Experiments 2 and 3, as well as Experiment 5 that will be described later in this section.

At $t=0 \text{ min}$, absolute resistivities in the areas of pre-existing cavities range from $32\text{--}40 \text{ }\Omega\cdot\text{m}$, considerably lower than in the pre-flow images from Experiments 2 and 3. This indicates that infiltration had already occurred, filling these cavities with soil particles and water prior to the first measurement in Experiment 4.

A key feature of Experiment 4’s ratio images is the pronounced red coloration across the graph, while blue areas remain faint and limited, suggesting minimal additional water content increase in the subsoil throughout the experiment. Pale blue patches begin to emerge at $t=22 \text{ min}$ and gradually intensify at a slow rate until the end of the experiment. In contrast to Experiments 2 and 3, these patches extend through the entire depth of the focus area, including depths of $0.26\text{--}0.6 \text{ m}$, indicating that at this higher flow discharge, deeper infiltration occurs. This trend was absent in the earlier experiments where flow discharges were lower.

The prevalence of red areas in Experiment 4 suggests active void development, likely driven by the increased flow discharge, which may have induced higher pore pressures in the subsoil. This, in turn, could lead to the expansion of pre-existing cavities and the formation of new voids. Further quantitative analysis of water content in the subsoil before and after overflow runs would be necessary to confirm the link between increased flow discharge and void formation.

While void formation patterns in Experiment 4 align only partially with those observed in Experiments 2 and 3, some similarities are present. In Experiments 2 and 3, voids appeared consistently at $X=1.7\text{--}2.1 \text{ m}$, $X=4.1\text{--}4.3 \text{ m}$ and $X=4.9\text{--}5.1 \text{ m}$. In Experiment 4, however, only the void at $X=1.7\text{--}2.1 \text{ m}$ reappears, starting at $t=10 \text{ min}$. Additionally, similar to Experiment 3, red spots emerge at the top layer of the subsoil from $t=10 \text{ min}$, upstream of the void formation,

specifically at $X=2.1-3.2$ m. These spots gradually spread across the top layer, likely signaling surface erosion initiation as observed in Experiment 3.

At the end of Experiment 4, a marked resistivity increase occurs across the entire top layer when the flow ceases. This sharp rise suggests a rapid transition in the top layer, as water-filled gaps created under high pressure are quickly replaced by air, likely due to the drop in pore pressure post-flow.

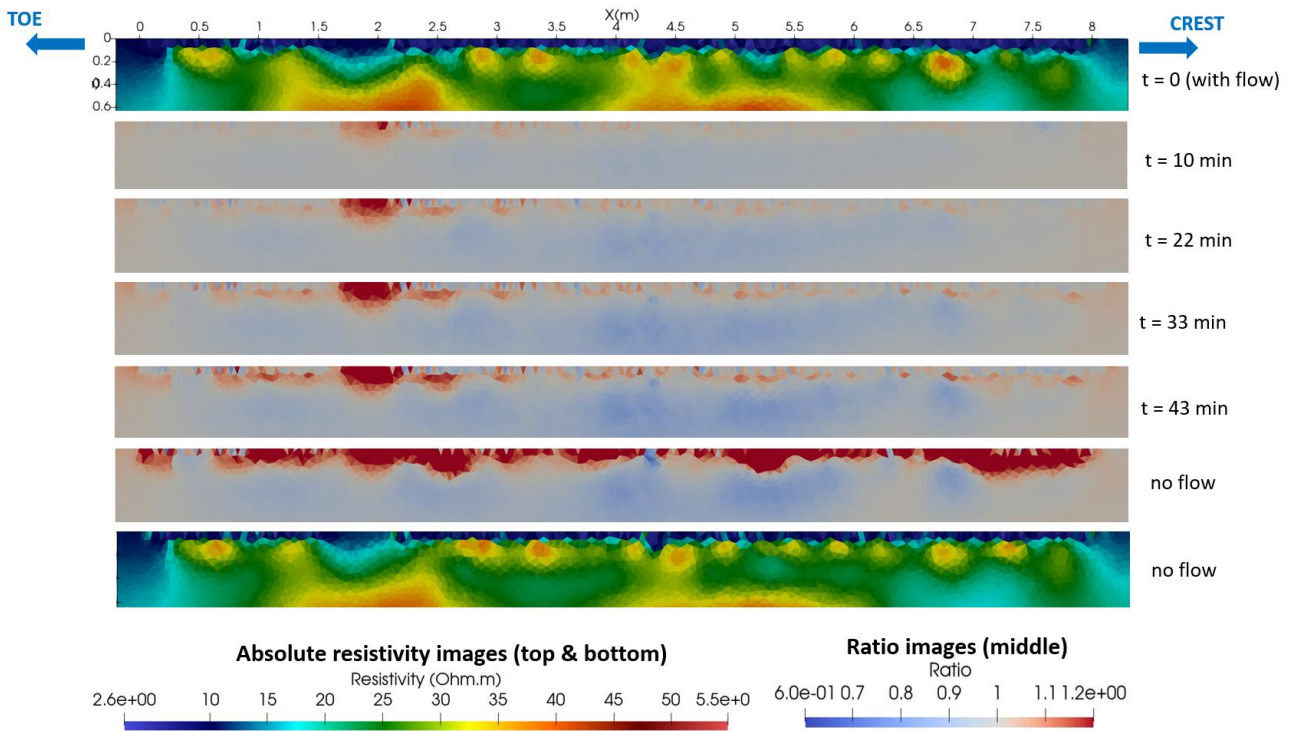


Figure 12: Measurements for experiment 4, cable 1, with a reference point for the ratio images after the flow started.

Experiment 5 (Figure 13), conducted immediately after Experiment 4, used the highest flow discharge achievable by the pumping system ($q=12$ m³/min). Having as a reference a state of non-flow, the results appear notably different than those of Experiment 4 despite the fact that both experiments used much higher flow discharges than experiments 2 and 3. Unlike Experiment 4, where void creation dominated the resistivity patterns, Experiment 5 is characterized by prominent infiltration across the subsurface.

In the ratio images, blue spots indicating increased water content are clearly visible in the top layer of the subsoil. Dark blue regions are particularly pronounced at locations $X=2.3-2.7$ m, $X=4.7-5.4$ m and $X=6.7-8$ m, all of which correspond to pre-existing voids. Specifically, the regions at $X=2.3-2.7$ m and $X=4.7-5.4$ m align with pre-existing mole cavities, while the region at $X=4.7-5.4$ m coincides with the location of a newly formed void from the first experiment. The low resistivity values of these dark blue spots suggest that the voids have become filled with water in this experiment, confirming ongoing infiltration.

It is noted that the ratio images remain almost unchanged throughout the course of Experiment 5. The only significant alteration is the appearance of a small red spot at $X=2.1$ m, indicating a slight expansion of nearby cavities. This overall stability may suggest that the slope has reached a temporary equilibrium, where further significant changes in the subsoil conditions could only occur with a sudden shift in flow discharge or a considerable extension of the experiment duration. This hypothesis warrants further investigation into the internal erosion processes to better understand the long-term behaviour of such systems. Among others it needs to be investigated whether the road plates that were installed on the top of cable 1 played a role in reaching this temporary equilibrium, by reducing the flow on the soil surface and the flow velocities.

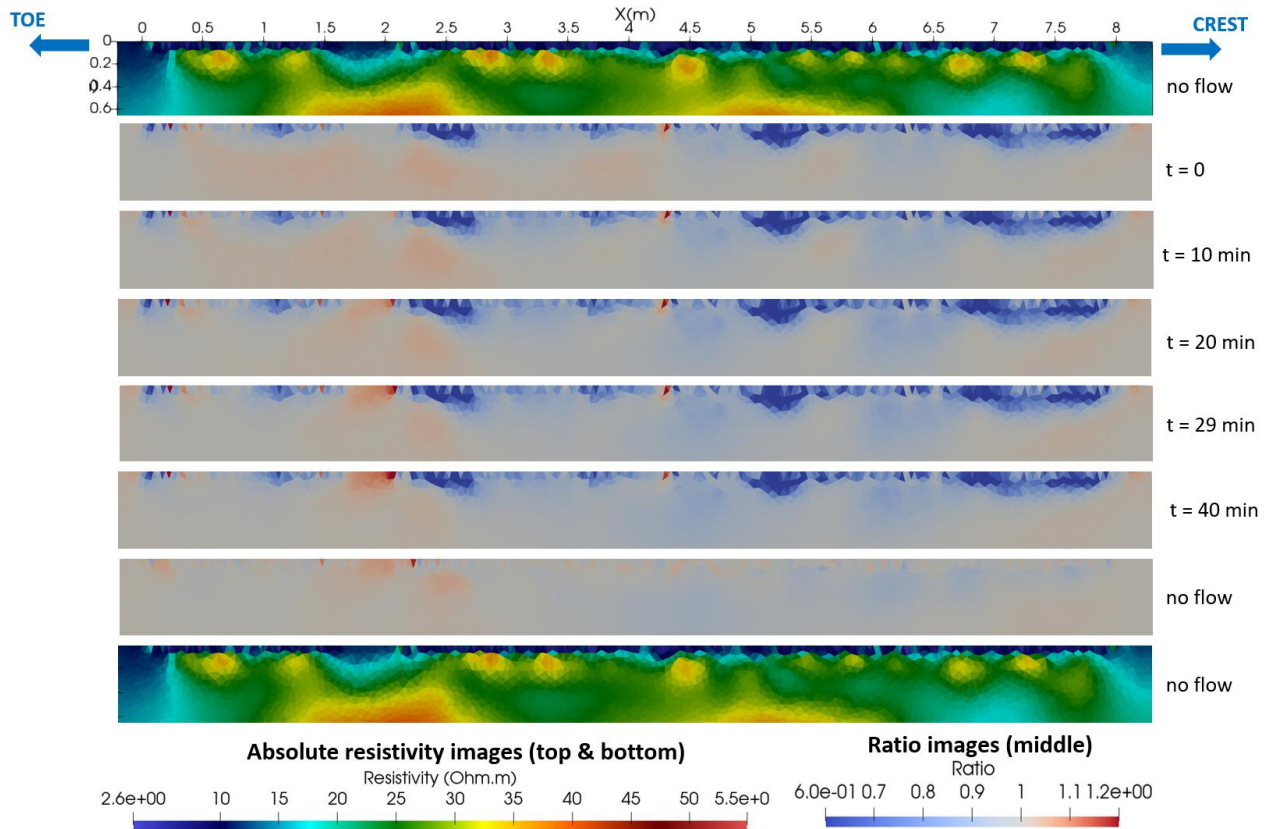


Figure 13: Results of ERT experiment 5, cable 1.

4.3 Interpretation of results

The resistivity values measured during the experiments ranged from $2.6 \Omega \cdot m$ to $55 \Omega \cdot m$, corresponding to varying levels of water saturation and air-filled voids. The lowest resistivity values (around $2.6 \Omega \cdot m$) are associated with highly water-saturated zones, where water completely fills the soil pores, increasing conductivity. These areas consistently appeared in the upper 10 cm of soil, reflecting the initial wet conditions due to rainfall and subsequent saturation from the overflow tests. In contrast, the highest resistivity values (up to $55 \Omega \cdot m$) were indicative of air-filled voids, such as those created by mole burrows. As observed in Figures 9 to 13, these high-resistivity regions were initially concentrated around known mole burrow locations but diminished as water infiltrated and filled the cavities over the course of the experiments.

In the early experiments (2 and 3), resistivity ratio images revealed the formation of new voids adjacent to pre-existing mole cavities, evidenced by the appearance of red regions in the images that indicate increased resistivity. However, at Experiment 2, as the experiment progressed, the newly formed voids were gradually filled with water and soil particles, as reflected in the transition from red to grey hues. This transition suggests that under moderate flow discharges ($\leq 5.8 m^3/min$), the soil retained the capacity to refill voids with infiltrating water and soil particles, preventing extensive void expansion.

The results of Experiments 4 and 5, conducted with higher flow discharges (9 and $12 m^3/min$), further illustrate the influence of hydraulic conditions on subsurface processes. In Experiment 4, the increased flow discharge led to deeper infiltration, as seen in the resistivity changes extending to depths of 60 cm. The pronounced red coloration across the ratio images indicates substantial void development at both shallow and deeper depths, suggesting that higher flow discharges increased pore pressures, driving the formation of new cavities and the expansion of existing ones. Additionally, the appearance of red spots near the surface aligns with surface erosion processes, likely initiated by water displacing surface materials and uprooting vegetation. It is noted that the area was covered with road plates, which in principle are expected to have reduced the intensity of erosion, both internal and on the surface.

Experiment 5, conducted immediately after Experiment 4 at the maximum achievable flow discharge, exhibited a contrasting pattern. Rather than further void formation, the ratio images indicated widespread infiltration across the subsurface, with prominent blue regions corresponding to increased water content within pre-existing cavities. The stability of the ratio images throughout this experiment suggests that the soil had reached a state of equilibrium, where further significant changes in subsurface conditions could not be induced without altering the flow discharge or extending the experiment's duration. This stability highlights the potential for a self-limiting erosion process under certain hydraulic conditions, where water-filled voids resist further expansion due to reduced pore pressure gradients.

The pre-existing mole tunnels played a significant role in directing water infiltration and void expansion throughout the experiments. The alignment of high resistivity regions with known mole burrow locations in the pre-experiment scans, and the subsequent decrease in resistivity at these points, indicate that these air-filled tunnels acted as pathways for water infiltration. Over time, the tunnels were filled with water, reducing resistivity and mitigating the risk of further void expansion. However, in Experiments 4 and 5, where higher flow discharges were applied, the persistence of red regions at specific mole tunnel locations (e.g., $X = 1.7\text{--}2.1$ m) suggests that some tunnels remained resistant to full infiltration, potentially acting as pressure relief zones that could localize void formation.

The surface erosion observed in Experiments 3 and 4, indicated by high-resistivity spots near the surface, is another key process influenced by flow discharges. The formation of small voids near the surface, likely caused by the uprooting of surface vegetation and displacement of soil, was a recurring phenomenon in these experiments. The gradual disappearance of these spots over time suggests that surface erosion occurs rapidly at the onset of high-flow events but stabilizes as surface materials are either eroded or compacted. In contrast, deeper subsurface changes, particularly void expansion, were more persistent under higher flow conditions, as seen in Experiment 4, where new voids continued to develop throughout the experiment.

The consistent resistivity patterns observed in Experiment 5, along with the limited changes in subsurface conditions, suggest that the levee slope may reach a temporary state of equilibrium under sustained high-flow conditions. This finding raises important questions about the long-term stability of such systems. However, this finding is influenced by the presence of road plates, which significantly reduce the direct flow on and into the soil. The road plates lead to lower flow velocities and, consequently, much less erosion compared to scenarios without such protection. Without the road plates, we would expect higher velocities and increased erosion, potentially altering the observed resistivity patterns and stability outcomes. This highlights the critical role of surface protection in mitigating erosion processes. While short-term experiments may show minimal changes after a certain threshold, prolonged exposure to high flow discharges or intermittent flow events could lead to gradual weakening of the subsurface, especially if voids remain partially filled with air, as seen in some regions of the levee. Further investigation into the long-term behavior of internal erosion processes, especially under varying protective conditions, is necessary to better understand the thresholds at which sudden structural failures may occur.

5 Discussion

5.1 Feasibility of ERT as a monitoring technique for large-scale experiments

This study highlights Electrical Resistivity Tomography (ERT) as a powerful, non-destructive technique for monitoring subsurface changes during large-scale levee overflow experiments. ERT's ability to image subsurface features in detail is critical for understanding how structures, such as pre-existing animal burrows, influence levee stability during high-flow events. In this study, ERT identified low resistivity zones associated with high water saturation and high resistivity zones linked to air-filled voids. These results aligned with on-site observations and corroborated findings from ground-penetrating radar, supporting ERT's ability to detect subsurface features that could compromise structural integrity under overflow conditions. Additionally, time-lapse ERT proved valuable in capturing resistivity changes linked to crucial processes like soil displacement and internal erosion around burrows, which are otherwise challenging to monitor with surface-level inspections alone.

ERT is considered a non-invasive and non-destructive geophysical technique because it does not require excavation or the removal of soil. During surveys, stainless steel electrodes (or pins) are inserted into the ground at shallow depths, typically about 10–15 cm, with a diameter of approximately 2–3 cm. These small electrodes are placed carefully to ensure minimal disruption to the soil structure and ecosystem. Since the pins are shallowly embedded, their removal leaves minimal impact on the soil. Small holes created by the pins generally close naturally due to the soil's cohesion and moisture content, preserving the integrity of the surface. This ensures that the method remains environmentally safe, providing valuable subsurface data without lasting effects on the soil's physical or chemical properties.

ERT protocols in this study combined shallow measurements in small time intervals with deeper measurements in longer time intervals, effectively capturing both surface and subsurface changes across different experimental conditions. Protocol adjustments were possible during the experiments, demonstrating ERT's adaptability in dynamic field environments, and highlighting its suitability for real-time, in-situ applications.

In this study, ERT monitoring was conducted on a levee section covered with synthetic road plates, which is an atypical condition in erosion testing, where non-covered slopes are typically prioritized. The road plates altered the hydraulic loading and erosion processes by eliminating the shear stress that water would typically exert on the grass surface beneath them. This reduction in surface erosion likely decreased the magnitude and severity of internal erosion beneath the plates. Such load-reduction capability is one of the reasons road plates are considered a potential emergency measure during high-water events.

Quantifying the exact extent to which the road plates mitigated internal erosion requires further research. Ideally, future experiments should compare levee sections with similar designs and conditions, both with and without road plates, to isolate the plates' effect. However, such experiments are logistically challenging and rare, making it difficult to conduct such a study in the short term. It is worth noting that a similar rigid covering was used during the Polder2C's project on another test section. In that experiment, a pre-existing scour hole (approximately 1.5×1.5 m in surface area and 50 cm deep) was covered with plywood and a plastic foil lining before being subjected to overtopping. The hydraulic load in that test was significantly higher than in our overflow experiment, with flow velocities reaching up to four times greater than the maximum velocities in our study. Despite these higher hydraulic loads and the vulnerable initial conditions, the rigid covering effectively mitigated further erosion. This evidence supports the conclusion that rigid coverings like road plates can provide reasonable protection against erosion during high-water events. While road plates may be less robust than the plywood-plastic covering used in the Polder2C's experiment, their performance under lower hydraulic loads demonstrates their potential utility. While the road plates likely reduced the magnitude of surface erosion, they did not entirely prevent internal erosion processes, as evidenced by the resistivity changes observed during the experiments. This confirms the ability of the ERT system to monitor internal erosion dynamics even under these conditions.

The road plates provided a significant advantage for performing high-resolution ERT measurements by enabling continuous data collection during active flow conditions. This allowed us to create a dense time series of resistivity measurements (every 3–6 minutes), capturing the internal dynamics in real time. However, we acknowledge that there are alternative methods for securing the electrodes that could allow resistivity measurements during flow without the need for road plates. For example, stronger mounting points at the beginning of the cable and pins soldered directly to the cable could ensure that electrodes remain securely in place even under high flow velocities. Another possibility would involve suspending the pins from a platform, with the cable suspended in the air and the platform's feet positioned outside the flow area. This design could weigh around 10 kg and would be relatively straightforward to implement. A third scenario involves operating the system under continuous flow conditions with the cable fully submerged. In such cases, the pins may not be necessary, as the current can flow directly from the submerged cable to the ground. The primary function of the pins is to inject current into the ground in configurations where the cable takeout is above the surface.

To address the influence of the road plates on subsurface dynamics, we recommend further research into alternative electrode configurations and sensor coverings that minimize interference with the hydraulic and erosion processes. A promising approach could involve flexible, watertight coverings such as ethylene propylene diene monomer (EPDM) foil. Small EPDM patches (e.g., 25–50 cm²) could be used to cover individual sensors, isolating them from the flow while allowing measurements during overflow. These patches could be pinned to the ground in a manner similar to the road plates but with reduced interference on surface erosion. A potential challenge with this approach is that securing the EPDM patches would likely require metal pins placed closer to the sensors than in the current setup, which could introduce noise in the resistivity measurements. To address this, synthetic pins could be explored as an alternative. Further research

is needed to optimize the configuration to ensure minimal noise while maintaining negligible interference with subsurface dynamics.

In summary, the presented ERT monitoring system offers valuable insights into internal erosion processes during overflow, even with the limitations posed by the road plates. The dense time series of resistivity measurements provides a unique capability to observe the progression of infiltration and cavity expansion under realistic testing conditions. While alternative setups such as improved electrode mounting or flexible coverings could enhance applicability, we believe the current findings demonstrate the system's significant utility and potential for advancing the understanding of internal erosion processes.

Despite its advantages, ERT faces limitations in real-time overflow monitoring. Environmental factors, such as interference from metal objects, temperature variations, and rainfall, can introduce noise and affect data accuracy. Electrode spacing, array configuration, and coupling quality also influence resolution; inadequate setups may reduce sensitivity to deeper or smaller anomalies, especially in complex and uncontrolled field conditions. While the cables are robust to weather and overflowing water, in cases where severe flow speeds are expected, even safer pin installations might be considered. To overcome acquisition time limitations, future experiments could use systems with more channels (e.g., 12 or more compared to the 8-channel system we used) to increase the number of data points per current injection. Alternatively, multiple systems could be deployed at adequate distances from each other (typically at least four times the depth of investigation) to avoid interference. Furthermore, ERT's reliance on 2D imaging limits its ability to represent the 3D complexity of evolving subsurface cavities accurately, particularly in detecting irregular or expanding features like animal burrows. Integrating ERT with complementary techniques, such as ground-penetrating radar, may improve detection accuracy by providing a more comprehensive subsurface view.

5.2 Reliability of ERT results

The results indicate that ERT can reliably capture subsurface responses to overflow events, making it a valuable tool for monitoring levee stability. ERT's sensitivity to hydraulic-driven changes, observed in resistivity responses across different flow discharges (5.6 to 12 m³/min), emphasizes its potential for detecting indicators of subsurface instability, such as deeper water infiltration and cavity expansion under elevated flow conditions. This capacity to detect critical subsurface changes reinforces ERT's utility for real-world levee safety applications.

ERT's ability to capture signs of temporary stabilization, as seen in the apparent equilibrium during Experiment 5, suggests it may be able to differentiate between self-limiting erosion and ongoing degradation risks. Future research should explore ERT's effectiveness in tracking cumulative subsurface changes over prolonged stress conditions, particularly as sustained high flow discharges could progressively weaken soil structures and heighten the risk of structural failure.

The effectiveness of ERT in detecting resistivity changes throughout the experiments demonstrates its value for levee monitoring, though several factors influence data reliability. A major challenge that needs to be addressed in future research is the assessment of the cumulative damage effect that can be expected when consecutive tests take place at the same levee section, which was the case in this study. Repeating overflow on a section that was subject to overflow earlier introduces complexities in distinguishing new erosion from pre-existing damage. When flow stops, the surface water pressure is removed, allowing the subsoil to partially settle between experiments, creating space for a temporary stabilization of the subsurface. The effect of this phenomenon on the overall erosion pattern is currently unknown.

To further validate the reliability of ERT results, future studies should consider integrating complementary methods and approaches. Benchmarking ERT measurements against independent techniques, such as ground-penetrating radar (GPR), time-domain reflectometry (TDR), or borehole logging, would help verify resistivity changes observed in the experiments. Additionally, the use of piezometers and moisture sensors near critical zones could correlate resistivity responses with direct measurements of water content and pore pressure, enhancing confidence in ERT interpretations.

Controlled laboratory experiments using scaled physical models of levees could provide direct correlations between ERT results and observed subsurface changes, such as infiltration rates, cavity formation, or soil erosion. Similarly, post-experiment field validation through pre-and post-excavation surveys could confirm the accuracy of ERT in identifying

zones of instability. Integrating ERT data with numerical models of water flow and soil stability offers another powerful validation method by simulating resistivity responses under controlled conditions.

Repeatability studies are essential for evaluating ERT data reliability. Repeating measurements under similar conditions would allow for statistical analysis, such as error quantification and confidence interval calculations, to assess the consistency of results. Cross-sectional and temporal correlation of resistivity changes could help differentiate between temporary and permanent subsurface changes, particularly in dynamic environments.

Post-experiment forensic analyses, such as excavation or soil coring, can validate predictions of subsurface changes made by ERT. Calibrating ERT systems before experiments using zones with well-defined subsurface properties can establish baseline resistivity responses, ensuring accurate interpretation of deviations during monitoring.

All the abovementioned validation approaches, including benchmarking against independent techniques, controlled experiments, numerical modeling, repeatability studies, and post-experiment analyses, require further research to fully establish their effectiveness and integration into standard monitoring practices. Additionally, further research is needed to better understand the influence of soil type, moisture content, and compaction on ERT measurements, particularly under repeated stress conditions. Investigating these factors will help address the complexities of distinguishing new erosion from pre-existing damage and improve ERT's utility for real-world levee safety applications.

5.3 Interpretability of results

Reductions in observed resistivity can be attributed not only to increased water content but also to soil deformation, such as the collapse of cavities. Soil deformation alters the pore structure, reducing air-filled voids and increasing water-filled pore connectivity, contributing to resistivity decreases. Distinguishing between these processes using ERT is challenging as both affect resistivity similarly, but three indicators could help. The first one is spatial patterns. Resistivity drops localized around known high-resistivity areas (e.g., mole burrows) may indicate cavity collapse. The second indicator is temporal trends. Rapid changes might indicate water infiltration, while slower changes may point to soil deformation. The third indicator is depth variations. Water infiltration affects shallow layers, while cavity collapse may show deeper changes. While ERT provides valuable insights, distinguishing specific mechanisms like cavity collapse requires additional validation methods. It is recommended that future studies focus on integrating ERT with other techniques that allow relevant validations.

While interpreting resistivity measurements, it is important to acknowledge factors such as surface vegetation. For instance, the grass cover and root system in the top soil layer could potentially influence resistivity measurements by introducing small-scale variations in soil structure, moisture retention, and ionic conductivity. However, in this study, these factors were considered to have minimal impact on the observed resistivity trends for several reasons. First because of the depth of measurement. The resistivity readings are influenced by the bulk soil properties over the entire measurement depth, extending beyond the root zone. Although grass roots can alter the very top soil layer, their influence diminishes deeper into the clay layer, which dominates the resistive properties. Second because the moisture distribution was relatively uniform. Controlled overflow tests using fresh water ensured consistent saturation patterns, limiting variability introduced by surface vegetation. Third, because of the scale of influence. The study focused on detecting significant resistivity changes associated with large-scale features like saturated zones and voids, making the effects of grass and roots negligible in comparison.

The interpretability of ERT results would benefit from the use of clear, quantitative metrics indicating erosion rates and subsurface change. Presenting such metrics, like resistivity change rates, could make data interpretation more straightforward for experts assessing levee stability. The choice of reference images for ratio analysis is also critical. In Experiment 4 for example, the reference images differed from those used in other experiments. For Experiments 2, 3 and 5, it was possible to use 'dry state just before flow' as a reference, i.e. a so-called ' t_0 -image'. For Experiment 4, this was not possible, so the first image available was used, i.e. a ' t_1 -image'. Using the t_1 -image however did provide some additional insights. While it was not possible to produce a t_0 -image for Experiment 4, it is possible to produce t_1 -images for Experiments 2, 3 and 5. These distinct reference images could provide unique insights into erosion progression, yet further investigation is needed to identify which reference points best illuminate subsurface processes for comparative purposes.

6 Conclusion

This study demonstrates ERT's effectiveness as a non-invasive technique for monitoring subsurface changes in large-scale levee overflow experiments. By capturing resistivity variations over time, ERT provides valuable insights into key levee processes, including water infiltration, soil stability, and erosion pathways. The technique's sensitivity to resistivity changes makes it particularly effective in identifying and tracking subsurface vulnerabilities, such as animal burrows, positioning ERT as a promising tool for levee stability assessment under simulated flood conditions.

In this study, ERT proved feasible, informative, and scalable for real-time levee monitoring in overflow scenarios. Its continuous resistivity measurements reveal critical patterns of water movement and soil stability under dynamic conditions, highlighting its potential as a reliable, ongoing monitoring method for levee and dam safety. However, further studies are recommended to examine the implications of long-term erosion and void stability to assess ERT's effectiveness in predicting structural vulnerabilities over extended periods.

Acknowledgements

The field experiments were made possible through the invaluable material support provided by the Dutch Regional Water Authority Brabantse Delta, which supplied the pump and road plates and assisted with their installation on the levee slope. The authors also extend their gratitude to the dedicated team at Flanders Hydraulics for their exceptional efforts in installing the flume on the levee and consistently monitoring the execution of the experiments. Their commitment and support were instrumental to the success of this work.

Funding

The support by the European Territorial Cooperation Programme Interreg 2 Seas 2014-2020 and the Domain of Technology, Water & Environment of HZ University of Applied Sciences are acknowledged.

Author contributions (CRediT)

VT: Conceptualization, Development of overall test plan, Funding acquisition, Data Analysis, Project administration, Supervision of experiment, Writing – original draft, review & editing.

MK: ERT cable configuration, Data collection plan, Data curation and processing, Visualization of results, Writing – original draft, review & editing.

RN & EA: Deployment of ERT system on the levee, Supervision of experiment and ERT data collection.

ARK: Conceptualization, Development of overall test plan, Supervision of experiment, Writing – original draft, review & editing.

AK: Conceptualization & Writing – review & editing.

Data access statement

The data acquired in the study will be made available on request.

Declaration of interests

The authors report no conflict of interest.

Abbreviations

ERT Electrical resistivity tomography

References

- Antoine, R., Fauchard, C., Guilbert, V., Beucamp, B., Ledun, C., Heinkele, C., Saussaye, L., Muylaert, S., Vancalster, W., Depreiter, D., and Sergent, P.: GEOPHYSICAL AND UAV-BASED OBSERVATIONS OVER A FLOOD DEFENSE STRUCTURE: APPLICATION TO THE POLDER2C'S EXPERIMENTAL DIKE, *Int. Arch. Photogramm. Remote Sens. Spatial Inf. Sci.*, XLIII-B3-2021, 237–242, <https://doi.org/10.5194/isprs-archives-XLIII-B3-2021-237-2021>, 2021.
- Bayoumi, A & Meguid, MA, 2011. Wildlife and safety of earthen structures: a review, *Journal of failure analysis and prevention* 11(4):295-319. <https://doi.org/10.1007/s11668-011-9439-y>
- Bulckaen, D., Smets, S., De Nocker, L., Broekx, S. & W. & Dauwe, W, 2006. Updating of the Belgian Sigma plan on a risk-assessment basis. In: *Floods, from defence to management*, Francis, Leiden, Netherlands, ISBN 0415391202.
- Davies, MCR, Bowman, ET & White, DJ, 2010. Physical modelling of natural hazards. In: Springman, S., Laue, J., & Seward, L. (Eds.). (2010). *Physical Modelling in Geotechnics*, Two Volume Set: Proceedings of the 7th International Conference on Physical Modelling in Geotechnics (ICPMG 2010), 28th June - 1st July, Zurich, Switzerland (1st ed.). CRC Press. <https://doi.org/10.1201/b10554>
- Camici, S, Barbetta, S & Moramarco, T, 2017. Camici, S, Barbetta, S. & Moramarco, T, 2017. Levee body vulnerability to seepage: the case study of the levee failure along the Foenna stream on 1 January 2006 (Central Italy). *Journal of Flood Risk Management* 10(3):314-325. <https://doi.org/10.1111/jfr3.12137>
- Cantré, S, Olschewski, J, Saathoff, F, 2017. Full-scale flume experiments to analyze the surface erosion resistance of dike embankments made of dredged materials, *Journal of Waterway, Port, Coastal, and Ocean Engineering* 143(3), 04017001. doi: 10.1061/(ASCE)WW.1943-5460.0000375
- Ceccato, F & Simonini, P, 2023. The effect of heterogeneities and small cavities on levee failures: the case study of the Panaro levee breach (Italy) on 6 December 2020, *Journal of Flood Risk Management*, e12882. <https://doi.org/10.1111/jfr3.12882>
- Depreiter, D & Peeters, P, 2020. Polder2C's, Overflow Test Plan Winter 2020-21; EU Interreg 2 Seas Project Polder2C's: Antwerp, Belgium, 2020. www.polder2cs.eu

- Depreiter, D & Peeters, P., 2021. Polder2C's, Overflow Test Plan Winter 2021-22; EU Interreg 2 Seas Project Polder2C's: Antwerp, Belgium, 2021. www.polder2cs.eu
- Dezert, T, Fargier, Y, Palma Lopes, S & Cote, P, 2019. Geophysical and geotechnical methods for fluvial levee investigation: a review, *Engineering Geology* 260. <https://doi.org/10.1016/j.enggeo.2019.105206>
- Government of the Netherlands, 2022. National Water Programma 2022-2027
- Hoffmans G, Akkerman GJ., Verheij H, Van Hoven A & Van der Meer J, 2008. The erodibility of grassed inner dike slopes against wave overtopping, *Coastal Engineering* 2008, pp 3224-3236. https://doi.org/10.1142/9789814277426_0267
- Hughes SA, 2011. Adaptation of the levee erosional equivalence method for the hurricane storm damage risk reduction system (HSDRRS). Tech. rep., U.S. Army Engineer Research and Development Center - Coastal and Hydraulics Laboratory, Vicksburg, Missipi, USMississippi, US
- Karaoulis M, Revil A, Werkema DD, Minsley BJ, Woodruff WF, Kemna A. 2011. Time-lapse three-dimensional inversion of complex conductivity data using an active time constrained (ATC) approach, *Geophysical Journal International*, Volume 187, Issue 1, October 2011, Pages 237–251, <https://doi.org/10.1111/j.1365-246X.2011.05156.x>
- Karaoulis, M, Revil, A, Tsourlos P, Werkema, DD & Minsley, BJ. 2013. IP4DI: a software for time-lapse 2D/3D DC-resistivity and induced polarization tomography, *Computers & Geosciences* 54:164-170. <http://dx.doi.org/10.1016/j.cageo.2013.01.008>
- Karaoulis, M., Tsourlos, P., Kim, J.-H., JH, Revil, A. 2014. 4D time-lapse ERT inversion: introducing combined time and space constraints. *Near Surface Geophysics*, 12 (1). 25-34. doi:10.3997/1873-0604.2013004
- Keirsebelik H, Tsimopoulou V, Lanzafame R, Van Putte N, Koelewijn A, Rikkert S, De Kleyn T & Schoelynck, J., 2024. Assessing the extent and connectivity of animal burrows using smoke: a practical tool for levee inspections, *Journal of Coastal and Riverine Flood Risk* , 3. <https://doi.org/10.59490/jcrfr.2024.0012>
- Koelewijn AR, De Vries G, Van Lottum H, Förster U, Van Beek VM & Bezuijen A., 2014. Full-scale testing of pipng prevention measures: Three tests at the IJkdijk, *Proc. Physical Modeling in Geotechnics*, Vol. 2, pp 891-897.
- Koelewijn AR, Rikkert SJH, Peeters P, Depreiter D, vanVan Damme M & Zomer W., 2022. Overflow Tests on Grass-Covered Embankments at the Living Lab Hedwige-Prosperpolder: An Overview. *Water*. 2022; 14(18):2859.
- Le HT, Verhagen HJ, Vrijling JK, 2017. Damage to grass dikes due to wave overtopping. *Natural Hazards* 86(2):849–875, DOI 10.1007/s11069-016-2721-2
- Le HT, Van der Meer JW, Schiereck GJ, Cath VM & Van der Meer, G, 2010. Wave Overtopping Simulator Tests in Vietnam. *ASCE, Proc. ICCE 2010*, Shanghai.
- Lengkeek HJ, 2022. Testing and modeling of sheet pile reinforced dikes on organic soils, Insights from the Eemdijk full-scale failure test, PhD thesis, TU Delft. doi: 10.4233/uuid:78df5e2b-740e-4268-a821-ed0ccea93e5
- Loke MH, 1994, The inversion of two-dimensional apparent resistivity data. unpubl. Ph.D. thesis, Un. of Birmingham (U.K.).
- Loke, M.H. andMH & Dahlin, T., 2002. A comparison of the Gauss-Newton and quasi-Newton methods in resistivity imaging inversion. *Journal of Applied Geophysics*, 49, 149-162.
- Nicaise S, Picault, C, Chaouch N, Byron F, Grémeaux Y, Doghmane A, Crampette F, Golay F & Bonelli S, 2023. In-situ overflow tests on a Rhone dike, proceedings 4th meeting of the European working group on overflow and overtopping erosion, Lyon, July 5-7.
- Orlandini S, Moretti, G & Albertson, JD, 2015. Evidence of an emerging levee failure mechanism causing disastrous floods in Italy, *Water resources research* 51:7995-8011. <https://doi.org/10.1002/2015WR017426>
- Ponsioen L, Van Damme M, Hofland B & Peeters P, 2019. Relating grass failure on the landside slope to wave overtopping induced excess normal stresses, *Coastal Engineering*, Elsevier, Vol 148 pp 49-56. <https://doi.org/10.1016/j.coastaleng.2018.12.009>
- Revil, A, Karaoulis, M, Johnson, T & Kemna, A, 2012. Review: some low-frequency electrical methods for subsurface characterization and monitoring in hydrogeology, *Hydrogeology Journal* 20:617-658, doi: 10.1007/s10040-011-0819-x
- Rosas Carbajal, M. 2014. Time-lapse and probabilistic inversion strategies for plane-wave electromagnetic methods. *Sciences of the Universe [physics]*. Université de Lausanne, 2014. English. NNT: tel-01095881

- Saghaee, G, Mousa, AA & Meguid, MA, 2017. Plausible failure mechanisms of wildlife-damaged earth levees: insights from centrifuge modeling and numerical analysis, *Canadian Geotechnical Journal* 54(10):1496-1508. <https://doi.org/10.1139/cgj-2016-0484>
- Sharp M, Wallis M, Deniaud F, Hersch-Burdick R, Tourment R, Matheu E, Seda-Sanabria Y, Wersching S, Veylon G, Durand E, Smith P, Forbis J, Spliethoff C, vanVan Hemert H, Igigabel M, Pohl R, Royet Pa, & Simm J, 2013. *The international levee handbook*. Construction Industry Research and Information Association (CIRIA), London, UK
- Steendam GJ, Peeters, P, Van der Meer J, Van Doorslaer K & Trouw K, 2013. Destructive wave overtopping tests on Flemish dikes, *Coastal Structures 2011*, pp 179-190. https://doi.org/10.1142/9789814412216_0016
- Taccari ML, 2015. Study upon the possible influence of animal burrows on the failure of the levee of San Matteo along the Secchia river, Modelling of groundwater flow with precipitation and water level changes and mechanism of collapse of the Secchia Failure with particular attention to burrows geometry and their influence to the stability of the dike (19th January 2014, San Matteo, Modena, Italy), MSc thesis, TU Delft, 13 July 2015, 160 pp.
- Tsimopoulou, V & Koelewijn A, AR, 2023. Management of harmful animal activities on levees: Fact finding fieldwork in the Living Lab Hedwige-Prosperpolder, Interreg 2Seas project Polder2C's. www.polder2cs.eu
- Van der Meer, JW, Hardeman, B, Steendam, GJ, Schüttrumpf, H & Verheij, H, 2010. Flow depths and velocities at crest and landward slope of a dike, in theory and with the wave overtopping simulator, *Coastal Engineering 2010*.
- Van Dijk, P.M., PM, 2021. Prediction method for grass erosion on levees by wave overtopping, linking models to experiments, MSc thesis, TU Delft.
- Victor L, Van der Meer JW & Troch P, 2012. Probability distribution of individual wave overtopping volumes for smooth impermeable steep slopes with low crest freeboard, *Coastal Engineering, Elsevier*, Vol 64, pp 87–101.
- Whitehead, E & Nickersons of Rothwell, 1976. A guide to the use of grass in hydraulic engineering practice, Technical note 71, CIRIA, London.
- Zwanenburg C, Den Haan EJ, Kruse GAM & Koelewijn AR., 2012. Failure of a trial embankment on peat in Booneschans, the Netherlands, *Géotechnique* 62(6):479-490.